ACS OMEGA

http://pubs.acs.org/journal/acsodf

Article

Optimizing Acetic Anhydride Amount for Improved Properties of Acetylated Cellulose Nanofibers from Sisal Fibers Using a High-Speed Blender

Romi Sukmawan, Kusmono,* and Muhammad Waziz Wildan

Cite This: *ACS Omega* 2023, 8, 27117−27126

Read Online

ACCESS | Metrics & More | Article Recommendations

ABSTRACT: Acetylated cellulose nanofibers (ACNFs) have shown a great potential for strengthening non-polar polymer matrices and better dispersion which can improve composite properties. However, insufficient acetylation may cause inadequate nanofibrillation ACNF during the fibrillation process. The objective of this work was to evaluate the effect of different amounts of acetic anhydride (0, 45, 55, and 65 mL) on the degree of substitution (DS), morphology, crystalline structure, and thermal properties of ACNF obtained from sisal fiber produced using a high-speed blender. The attenuated total reflectance-Fourier transform infrared spectroscopy revealed the success of the acetylation process by the presence of the carbonyl signal around 1724 cm^{-1}. Furthermore, the DS of ACNF was increased with the acetic anhydride amounts. X-ray diffraction analysis revealed that the crystalline structure of ACNF and non-ACNFs were cellulose I, and the crystallinity index of CNF was increased after acetylation treatment. Thermogravimetric analysis showed that the thermal stability of CNF was improved considerably after the acetylation process. The water contact angle of ACNF was higher than that of CNF, indicating that the structural property of CNF altered from hydrophilic to more hydrophobic after acetylation. In addition, the thermal resistance of CNF was improved significantly after acetylation treatment. The optimum amount of acetic anhydride was achieved in 55 mL of acetic anhydride (ACNF-55) which produced ACNF with a DS value of 0.5, a crystallinity index of 77%, a diameter of 87.48 nm, a maximum degradation temperature of 351 °C, and a contact angle of 37.7°. Overall, it was concluded that the obtained ACNF had great potential as reinforcement materials for nanocomposites based on non-polar polymeric matrices.

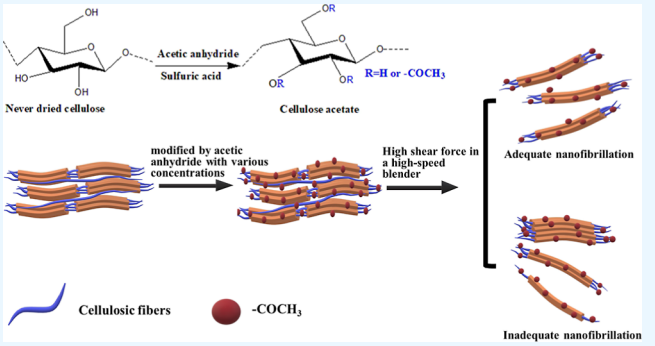

1. INTRODUCTION

Recently, cellulose nanofibers (CNFs) have received significant attention due to their excellent properties such as high strength and stiffness, high aspect ratio, very light, renewable ability, biodegradability, biocompatibility, high crystallinity, high surface activity, low toxicity, good rheological, and optical properties.[1−5] Because of their attractive advantages, CNFs have attracted increasing interest in many applications, including papermaking, coating additives, security paper, food packaging, gas barrier, and reinforcing agents in polymer nanocomposites.[6] CNFs are fabricated by the mechanical methods of cellulose-based materials, which are usually obtained after the removal of amorphous components such as hemicellulose, lignin, wax, and oils through chemical treatments.[7] The mechanical methods include high-pressure homogenization, micro fluidization, ultra-sonication,[8] high-speed disintegration,[9] and grinding.[10]

Although CNFs have excellent potential as a reinforcing agent in nanocomposites, as described above, it is difficult for CNF particles to be dispersed homogeneously in a non-polar polymer matrix, which makes the strengthening effect insignificant.[11] The hydrophilic behavior is ascribed to the hydroxyl groups on the surface of the cellulose fiber.[12] Therefore, to reduce the surface hydrophilicity of CNFs and improve their properties, it is necessary to carry out various surface modifications such as esterification, etherification, silylation, and organic acid grafting.[13,14] Among those modifications, acetylation is a commonly used surface modification in which the hydroxyl groups of cellulose are substituted by less hydrophilic acetyl groups.[15] Acetylation effectively reduces the number of hydroxyl groups in cellulose, thereby increasing the hydrophobicity and reducing hydrogen bonds.[16]

Received: March 31, 2023
Accepted: July 11, 2023
Published: July 20, 2023

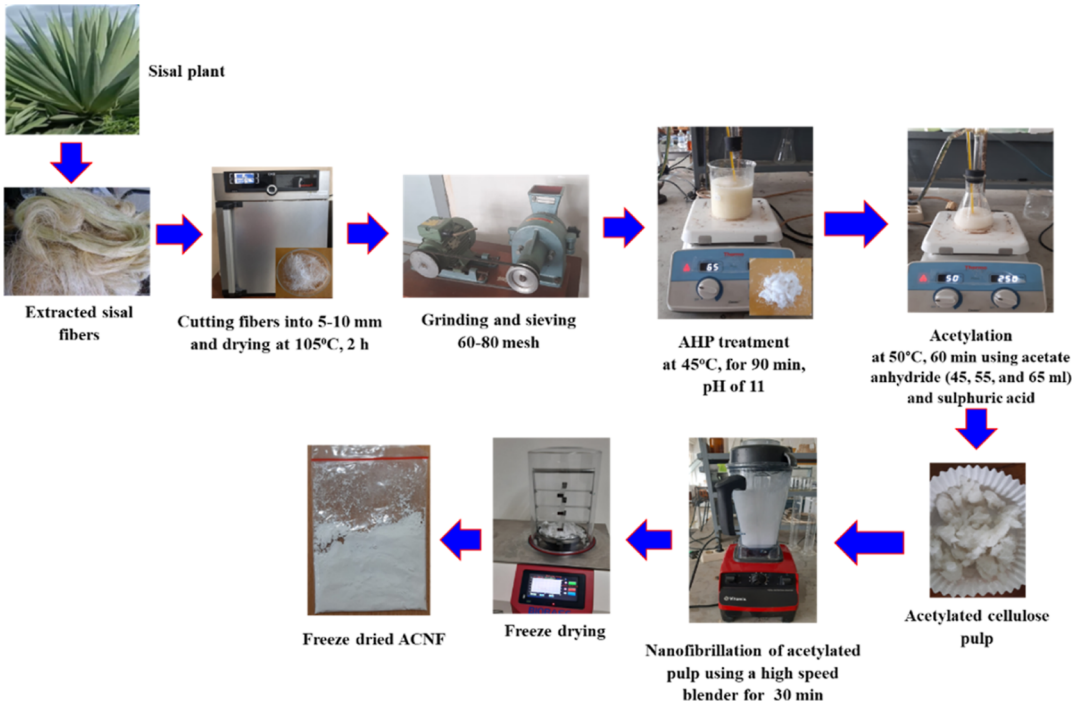

Figure 1. Extraction and isolation of ACNFs.

Numerous studies have been reported on the acetylation of CNFs isolated from different cellulose sources. The ACNF from the kenaf fibers was successfully prepared by Jonoobi et al.[17] and Ashori et al.[18] The ACNF from sisal fibers (SF) was also demonstrated by Trifol et al.,[19]where the SF were treated using alkali, bleached, and followed by acetylation. Zimmermann et al.[20] produced ACNF from microcrystalline cellulose (MCC) by acetylation treatment at 120 °C for 3 h and then followed by ultrafine grinding for 4 h. ACNF from cotton linter was reported by Yuan et al.[21] where acetylated cellulose nanofiber (ACNF) was prepared using a combination of acetylation and high-pressure homogenization for stabilizing Pickering emulsion. The properties of obtained ACNF are greatly affected by several factors, such as the type of cellulose sources, the molar ratios of acetic acid and acetic anhydride, the ratio of MCC to acetic anhydride, degree of substitution (DS), blending time, and the type and amount of ester groups.[16,22−24] Diop et al. investigated the effect of the acetic acid/acetic anhydride ratio on the properties of corn starch acetates.[22] They found that the ratio of acetic acid/acetic anhydride strongly influenced the crystallinity, surface morphology, water solubility, and water absorption index of corn starch, and the best ratio of acetic acid/acetic anhydride was achieved in 1:1. Zhou et al. demonstrated that the DS was increased with increasing the molar ratio of acetic anhydride/acetic acid.[16] Cheng et al. produced ACNF prepared from corn stalk MCC with different ratios of MCC to acetic anhydride using chemical-high-pressure homogenization processes.[23] They found that the DS was increased as the ratio of MCC to acetic anhydride increased. Moreover, the crystallinity index (C_rI) and thermal stability were decreased with increasing the ratio of MCC to acetic anhydride. Xu et al. successfully prepared acetylated cellulose nanocrystals via a one-step reaction with varying amounts of acetic anhydride from commercial MCC powder.[25] They demonstrated that both C_rI and DS were found to increase with increasing the acetic anhydride amounts.

In this work, SF were used as a source of cellulose to make CNFs because SF have a high cellulose content (60−70%)[26−28] and were widely available in the province of Nusa Tenggara Barat, Indonesia. Sisal fiber is extracted from the leaves of the *Agave sisalana* plant which is native to Mexico but can now grow rapidly in tropical countries around the world, including Indonesia. Therefore, it is very interesting to produce CNFs extracted from SF. To the best of the author's knowledge, no studies on the preparation of acetylated cellulose nanofibers (ACNFs) from SF using a high-speed blender with varying amounts of acetic anhydride have been reported. A high-speed blender was used in this work because it was proven to be effective in making CNFs with low energy consumption.[9,29,30]

In the present work, the ACNFs with different degrees of substitution were produced from the SF. The SF were first bleached using the alkaline hydrogen peroxide (AHP) solution. Then, the AHP-treated SF were modified using an acetylation process with different amounts of acetic anhydride, and the nanofibrillation was performed using a high-speed blender. The effect of the amounts of acetic anhydride on the characteristics of ACNFs was investigated in the present study. The characteristics of ACNF were evaluated using attenuated total reflectance-Fourier transform infrared (ATR-FTIR), X-ray diffraction (XRD), scanning electron microscope (SEM), thermogravimetric analysis (TGA), and the measurements of the DS and water contact angle.

2. EXPERIMENTAL SECTION

2.1. Materials. SF were obtained from Sumbawa Bangkit Sejahtera Inc., Nusa Tenggara Barat, Indonesia. The fibers were cultivated in West Nusa Tenggara Province, Indonesia, for a cultivation period of 2−3 years. The sulfuric acid (95−97%), glacial acetic acid (100%), acetic anhydride (>97%),

https://doi.org/10.1021/acsomega.3c02178
ACS Omega 2023, 8, 27117−27126

sodium hydroxide (NaOH), and hydrogen peroxide (30% in water) were bought from Sigma-Aldrich, USA. In addition, methanol (≥99%) and acetone (95%) were used as solvents. All reagents were analytical reagents and used directly.

2.2. Pre-Treatment of Sisal Fibers. Previously, ground (60−80 mesh) SF were soaked in distilled water for 2 h at 80 °C to remove any dirt and other soluble contaminants before the chemical treatment. Then, the fibers were bleached using AHP following the previous method with a slight modification.[26] Briefly, 10 g of the dried SF was added to 200 mL of an aqueous solution of both preheated 5 wt % H_2O_2 and 5 wt % NaOH at pH 11 and 45 °C for 90 min. The bleached pulp was washed with distilled water to a pH of 7.

2.3. Acetylation of Pre-Treated SF. The pulp of pre-treated SF was subsequently acetylated to produce hydrophobic CNFs. The acetylation process was conducted using never-dried (wet) cellulose. A total of 10 g of pulp was compacted manually between filter papers to reduce the moisture content as much as possible, followed by sequential solvent exchange using glacial acetic acid to displace water and lead to the hydroxyl groups being more accessible. The pressed pulp was initially soaked in a sequential solvent of 50 and 75 mL glacial acetic acid for 15 min every sequent and then filtered to remove the remaining solvent. The final step of the exchange process was soaking the filtered pulp into 100 mL glacial acetic acid for 60 min, followed by an acetylation process by adding different amounts of acetic anhydride (45, 55, and 65 mL) and sulfuric acid (0.2 mL) in a round-bottom flask with a flat base. The reaction was carried out under constant stirring at 50 °C for 60 min. The reaction was terminated by washing with distilled water several times, followed by methanol and acetone to remove any residual chemicals. The clean and wet acetate fibers were stored in sealed plastic bags at 5 °C until further use.

2.4. Nanofibrillation of Acetylated Cellulose Nanofibers. The ACNFs were fibrillated by a high-speed blender. There was 7 g of acetylated cellulose fibers put in 1000 mL of water and mixed using a high-speed blender (Vitamix TNC 5200, USA) at 37,000 rpm for 30 min. For comparison, untreated CNFs were also prepared with a high-speed blender. The three acetylated samples with 45, 55, and 65 mL acetic anhydride concentration and untreated CNFs are designed as ACNF-45, ACNF-55, ACNF-65, and CNF, respectively. ACNF and CNF suspensions were then freeze-dried to produce the dried ACNF and CNF powders. The extraction and isolation of ACNFs are demonstrated in Figure 1.

2.5. Characterizations. *2.5.1. ATR-FTIR.* The ATR-FTIR (IRAffinity-1S, Shimadzu, Japan) was used to compare changes in function groups between SF, CNF, and ACNF obtained at various amounts of acetic anhydride. The influence of amounts of acetic anhydride on the functional group alteration was evaluated. The spectra of the samples were recorded with an average of 34 scans and a spectral resolution of 4 cm^{-1} in the range of 400−4000 cm^{-1}.

2.5.2. DS. The DS of the samples was calculated using the FT-IR method as proposed by Barbosa et al.[31] The DS of the sample was determined by the normalization of the area of the absorbance peak of the ester at 1724 cm^{-1}, with the area under the absorbance peak of the cellulose unit centered at 1162 cm^{-1}. The DS was determined by the following eq 1

$$DS = \frac{A_{1724}}{A_{1162}} \quad (1)$$

where A_{1724} and A_{1162} are the areas under peaks of 1724 and 1162 cm^{-1}, respectively. Ten different sample positions of ACNF sheets were measured and the mean DS value was calculated.

2.5.3. XRD. The XRD characterization was carried out using an Empyrean X-ray diffractometer (Malvern PANalytical type of HR-XRD Empyrean DY 3831, Netherlands) using Cu Kα ray radiation (λ = 1,54 Å) operated at 40 kV and 30 mA. The spectra were recorded over the 2θ range of 10−40°, a step size of 0.02°, and a scan speed of 0.1°/min. In addition, the C_rI was determined by the Segal method,[32] according to eq 2

$$\%C_rI = \frac{I_{002} - I_{am}}{I_{002}} \times 100\% \quad (2)$$

where C_rI is the crystalline index, I_{002} is the maximum diffraction intensity for 2θ = 22−23° indicating the crystalline regions, and I_{am} is the intensity related to the amorphous regions at 2θ = 18−19°. The crystallite size (t) was determined following the Scherrer equation as in eq 3 below[33]

$$t = \frac{K\lambda}{\beta_{1/2}\cos\theta} \quad (3)$$

where K (0.91) is the Scherrer constant, λ (1.54060 Å) is the wavelength of radiation, $\beta_{1/2}$ is the full width at the half maximum of (200) diffraction peak in radians, and θ is the corresponding Bragg's angle.

2.6. SEM. The morphological structures of ACNF and CNF were observed using an SEM (JEOL Ltd., type of JSM-IT200 Electron Microscope, Japan) operating at 5 kV. Before SEM observations, the samples were sputter-coated with gold to avoid charging. Then, the CNF and ACNF diameters were measured based on the SEM images using the freely available ImageJ software. In this study, diameter measurements were made on 30 fibers at different locations on each SEM image and the average diameter was calculated.

2.7. TGA. The thermal behavior of the ACNF and CNF was evaluated by TGA (Hitachi STAA7300, Japan) by recording TGA and DTG curves. The measurements were conducted under a controlled atmosphere by placing about 12 mg of the sample in an aluminum pan and heating it to a range temperature of 30−600 °C at a heating rate of 10 °C/min under a nitrogen flow rate of 50 mL/min.

2.8. Water Contact Angle Measurement. The water contact angle was measured using a high-speed video camera (Fujifilm X-M1) with a speed of 6 fps and a shutter speed of 1/4000 s at room temperature. Approximately, 5 μL of distilled water was dropped on the sample, and the contact angle measurements were made 20 s after the drop touched the sample's surface. Three different sample positions were measured, and then the mean value was calculated.

3. RESULTS AND DISCUSSION

3.1. ATR-FTIR Spectroscopy. Figure 2 depicts the ATR-FTIR spectra of SF, CNFs, and ACNFs with various acetic anhydride concentrations. In the ATR-FTIR spectrum of SF, there were some visible peaks at 3449, 2897, 1725, 1590, 1162, 1037, and 892 cm^{-1}, respectively. The bands at 3449 and 2897 cm^{-1} corresponded to the stretching vibrations of the hydroxyl (−OH) groups and the C−H groups of cellulose, respectively.[34−38] The characteristic of the stretching vibrations of the carbonyl groups of acetyl and uronic esters of hemicellulose and ester bonds of carboxylic groups of ferulic and *p*-

https://doi.org/10.1021/acsomega.3c02178
ACS Omega 2023, 8, 27117−27126

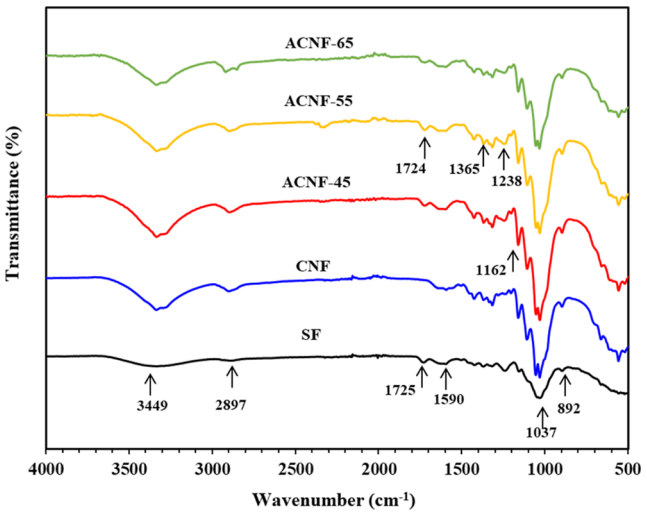

Figure 2. ATR-FTIR spectra of SF, CNF, ACNF-45, ACNF-55, and ACNF-65.

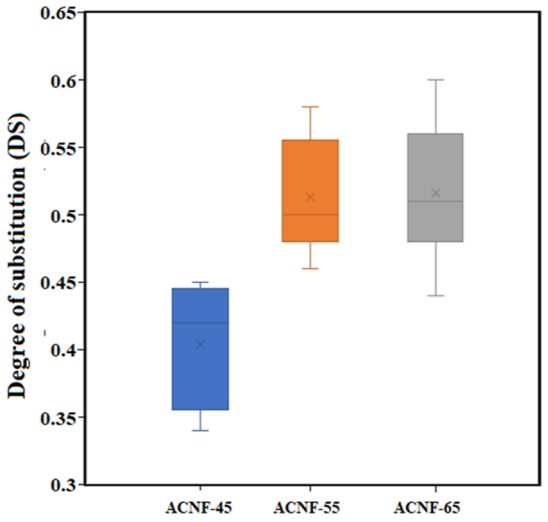

Figure 3. The effect of acetic anhydride amounts on DS.

coumaric acids of lignin was shown by a peak at 1725 cm^{-1}.[37,39,40] The band at 1590 cm^{-1} was related to the presence of COO− groups and corresponded to the stretching of the carboxyl group.[41] The band at 1162 cm^{-1} was ascribed to the stretching of C−O antisymmetric bridge groups. The pyranose stretching of C−O−C groups was revealed by the peaks at 1037 and 892 cm^{-1}.[42] Compared with the spectrum of SF, the CNF exhibited no peak at 1725 cm^{-1}, indicating the removal of amorphous components (hemicellulose, lignin, pectin, and wax) during the bleaching using the AHP. Three new peaks could be observed in the ATR-FTIR spectra of all ACNFs, namely at 1724, 1365, and 1238 cm^{-1}. The absorption bands at 1724, 1365, and 1238 cm^{-1} were attributed to the stretching of the carbonyl (C═O) groups, the methyl (CH_3) groups, and the acetyl (C−O) groups, respectively.[43−47] The appearance of three peaks confirmed the structural transformation due to the acetylation reaction. In other words, it was concluded that the acetylation of CNFs was successfully obtained. Moreover, the lack of any peaks at 1760 to 1850 and 1700 cm^{-1} indicated that the ACNF is free of acetic anhydride and the by-product of acetic acid. In other words, it was concluded that the acetylation of CNFs was successfully obtained. Figure 2 also shows no significant difference in the spectra of all ACNFs with different concentrations of acetic anhydride. This indicated that amounts of acetic anhydride did not affect the chemical structures of the ACNF. The same phenomenon was also reported by Ishida et al.,[48] where there are no significant differences in spectra of aqueous counter collision (ACC)-CNF by various wet surface acetylation.

3.2. DS Analysis. Figure 3 illustrates the DS value of ACNFs with different amounts of acetic anhydride. Figure 3 shows that when the acetic anhydride amounts were 45, 55, and 65 mL, the DS of ACNFs was 0.4 ± 0.04, 0.50 ± 0.04, and 0.52 ± 0.05, respectively. The results indicated that the DS increased with the amounts of acetic anhydride. The influence of the DS was associated with the reagent of the reaction slowly penetrating the crystal domains of cellulose, removing the hydroxyl groups in the crystalline area and more active acetyl groups involved in the acetylation process.[49] In the acetylation process, the role of acetic anhydride was shown to be more effective when the amounts of acetic acid were increased.[25] In this study, the highest DS obtained was 0.52 ± 0.05, indicating that the substitution of hydroxyl groups by acetyl groups was incomplete and the hydrogen bonding still existed between the anhydrous glucose units of the cellulose chains.[16] From Figure 3, it can also be seen that the relation between the amounts of acetic anhydride and the DS value was not linear. This trend suggested that the CNFs were heterogeneously acetylated by the procedure in this work.[1,16,50,51] In other words, this indicated that the acetylation process occurred increasingly from the surface to the cellulose core.[50,51] This result was consistent with previous reports.[16,51] An increase in the DS due to an increase in the amounts of acetic anhydride was also reported by Zhou et al.,[16] Colussi et al.,[52] and Duan et al.[53] However, the resulting ACNF had a lower DS than that reported by Duan et al.[53] which might be due to the limited degree of reaction on the wet cellulose surface in this study. The remaining water content on the cellulose surface makes it difficult for the hydroxyl groups to access during acetylation.

3.3. XRD Analysis. The XRD patterns of SFs, CNFs, and all ACNFs with different acetic anhydride concentrations are demonstrated in Figure 4. It can be seen from Figure 4 that the typical structure of cellulose I was exhibited by all samples. The characteristic peaks of cellulose I were shown by several peaks at 2θ values of 16°, 22−23°, and 34−35°, corresponding to (110), (200), and (004) planes, respectively.[46,54] It was revealed that the crystal structure of cellulose I remained during the bleaching using the AHP and acetylation process. These results were in agreement with previous studies.[21,55,56] Furthermore, the C_rI is calculated using Segal's empirical equation from the XRD patterns and their results are presented in Table 2. The C_rI values of SF and CNF were 50 and 58%, respectively. The result suggested that the CNF possessed a higher CrI than the SF. The increase in crystallinity was attributed to the removal of amorphous components, such as hemicellulose and lignin, within the SF during the bleaching with the AHP. These results were in agreement with the results reported by Sofla et al.[24] Furthermore, the C_rI values of the ACNFs under different acetic anhydride concentrations of 45, 55, and 65 mL were 74, 77, and 69%, respectively. Compared to the CNF, all ACNFs exhibited a much higher C_rI value (69−77%). The higher CrI value confirmed that the acetylation increased the C_rI of CNF considerably. The increase in crystallinity after acetylation was probably related

https://doi.org/10.1021/acsomega.3c02178
ACS Omega 2023, 8, 27117−27126

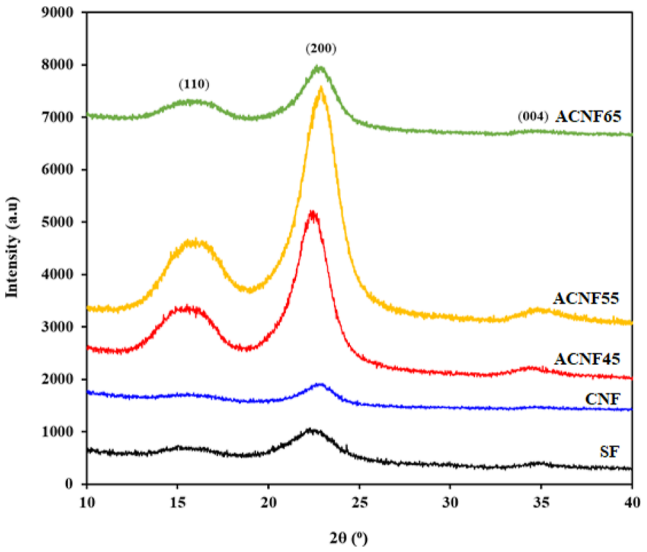

Figure 4. The XRD patterns of SF, CNF, ACNF-45, ACNF-55, and ACNF-65.

to the role of acetylation, which in addition to reducing the hydrogen-bond forces between cellulose molecules also removed amorphous components such as hemicellulose and lignin so that acetylation increased the C_rI. According to da Rosa et al.,[57] the acetylation process acts as a cleaning agent for inorganic compounds and amorphous domains in cellulose. As presented in Table 2, it was found that the C_rI value of the ACNF increased from 74 to 77% with increasing the acid anhydride concentration from 45 to 55 mL and then decreased to 69% when the acid anhydride increased further to 65 mL. These findings indicated that the optimal acetic anhydride concentration was achieved at 55 mL resulting in the highest CrI value. The highest C_rI value at an acetic anhydride concentration of 55 mL was associated with the most effective removal of residual amorphous domains in cellulose during acetylation. Furthermore, the reduction in CrI of the ACNF produced at an acetic anhydride concentration of 65 mL was attributed to partial damage to the crystalline structure of cellulose. All ACNFs had higher C_rI values than the results reported by Sofla et al.[24] and Duan et al.[53] The higher C_rI value in this study may be because the wet acetylation method reduces the effect of damage in the crystalline structure of cellulose during mechanical fibrillation compared with the dry acetylation method proposed by Sofla et al.[24] and Duan et al.[53] As shown in Table 1, the crystallite size of SF increased in the case of CNF and ACNF. Increasing crystallite size might be due to removing some amorphous parts of SF and recrystallization as the intermolecular force of attraction increases after several treatments.[58] The crystallite size of ACNF-55 and ACNF-65 was slightly reduced compared with

Table 1. Crystallinity Index and Crystallite Size of SF, CNF, ACNF-45, ACNF-55, and ACNF-65

sample	C_rI (%)	crystallite size (nm)
SF	50	2.9
CNF	58	4.0
ACNF-45	74	4.0
ACNF-55	77	3.9
ACNF-65	69	3.9

that of CNF and ACNF-45 after fibrillation with a high-speed blender. These findings demonstrated that fibrillation of acetylated pulp by a high-speed blender causes less damage to the crystalline structure of cellulose. Overall, it was concluded that the acetylation process unchanged the structure of cellulose I, and the acid anhydride influenced the C_rI of ACNFs.

3.4. SEM Observation. Figure 5 displays the SEM micrographs of CNF and ACNF under different acetic

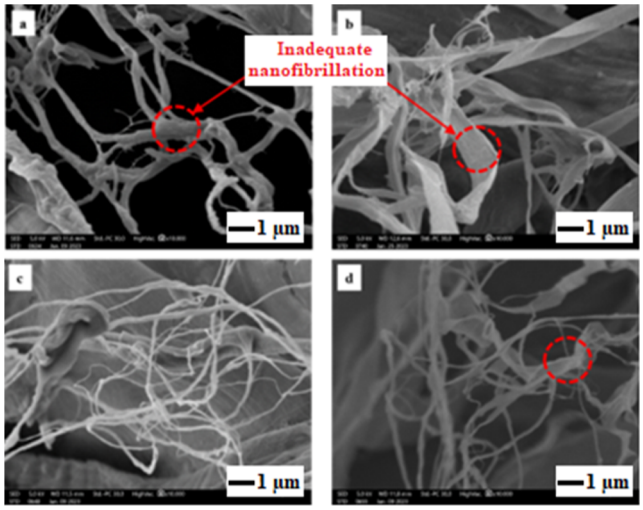

Figure 5. SEM images of (a) CNF, (b) ACNF-45, (c) ACNF-55, and (d) ACNF-65.

anhydride concentrations. Figure 5a–d illustrates the SEM images of CNF, ACNF-45, ACNF-55, and ACNF-65, respectively. As shown in Figure 5a, it can be observed that the CNF was partially fibrillated with an average diameter of 220.46 nm showing that the AHP treatment facilitated the fibrillation of fibers.[59] In addition, inadequate nanofibrillation, as presented by the red circle, was also observed in the CNF. The presence of inadequate nanofibrillation was also examined in the ACNF-45, as shown in Figure 5b. The inadequate nanofibrillation might be attributed to insufficient acetylation at 45 mL of acetic anhydride and a lower DS value of 0.5.[53] As presented in Figure 5c, a higher fibrillation rate, a more uniform size distribution and a smaller size were exhibited by ACNF-55. These phenomena indicated that hydrophobic modification has been advantageous to nanofibrillation during acetylation.[53]

Furthermore, the diameter distribution of CNF and ACNF with different acetic anhydride was measured using ImageJ processing software from SEM images and their results are demonstrated in Figure 6. The CNF had a diameter of 220.46 ± 115.42 nm, while the diameter of ACNF-45, ACNF-55, and ACNF-65 was 364.76 ± 282.12, 87.48 ± 49.76, and 132.13 ± 131.04 nm, respectively. Therefore, the average diameter of ACNF was in the order of ACNF-45 (364.76 nm) > ACNF-65 (132.13 nm) > ACNF-55 (87.48 nm). This suggested that the smallest diameter of ACNF was obtained at an acetic anhydride of 55 mL, attributed to the most effective acetylation process achieved at 55 mL of acetic anhydride. In other words, the degree of fibrillation reached a maximum at 55 mL of acetic anhydride, as indicated by the uniform diameter distribution of ACNF-55 without obvious inadequate nanofibrillation as presented in Figure 5c. The smaller diameter of

https://doi.org/10.1021/acsomega.3c02178
ACS Omega 2023, 8, 27117−27126

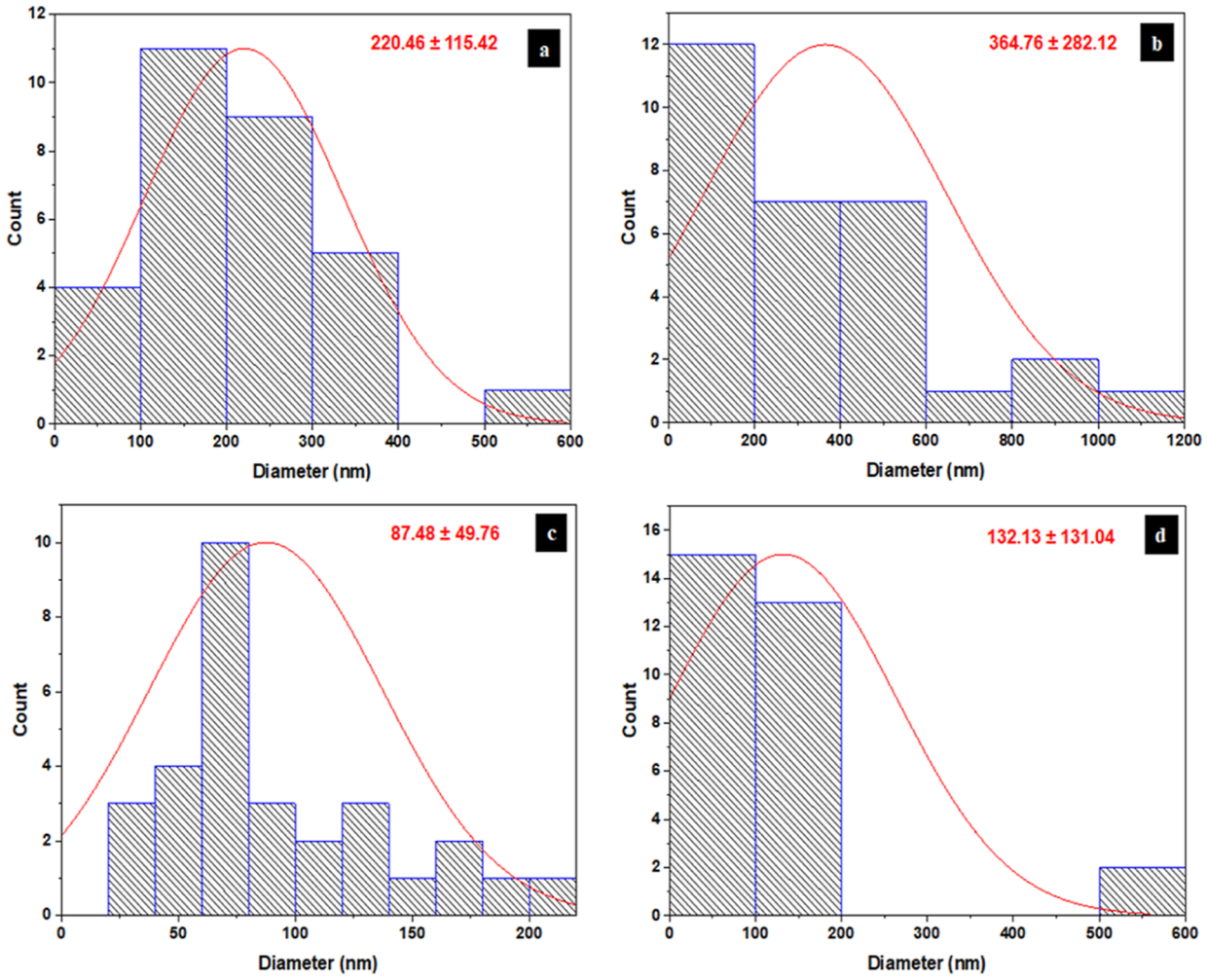

Figure 6. Diameter distribution of (a) CNF, (b) ACNF-45, (c) ACNF-55, and (d) ACNF-65.

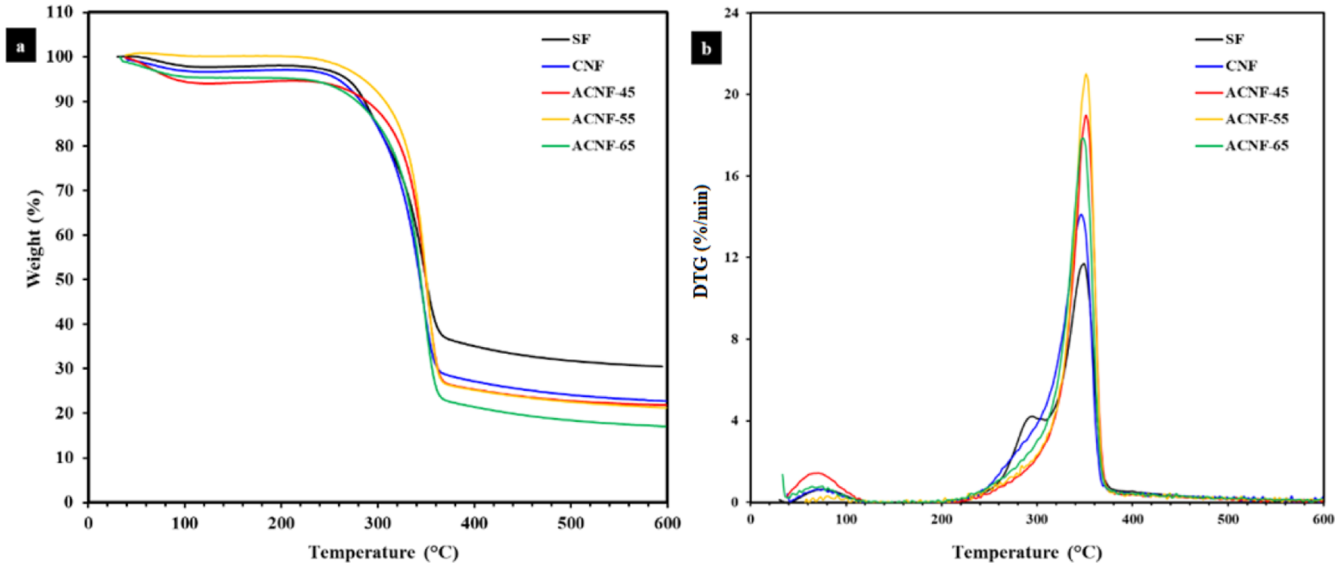

Figure 7. (a) TGA and (b) DTG curves of SF, CNF, ACNF-45, ACNF-55, and ACNF-65.

ACNF-55 and ACNF-65 compared to CNF was associated with the loss of the squared portion of the nanofiber during acetylation, which further decreased the overall size of the nanofiber diameter.[60] Moreover, deconstruction of the fiber cell wall structure during the acetylation process can lead to easier isolation of the nanofibers from the cell wall and lower levels of lateral aggregation due to the more hydrophobic surface of ACNFs.[61] The SEM analysis concluded that the

https://doi.org/10.1021/acsomega.3c02178
ACS Omega 2023, 8, 27117−27126

optimal acetic anhydride amount was achieved at 55 mL, resulting in the smallest size of ACNFs. The average diameter for the cellulose fibers produced from the ACNF-55 sample was comparable with the previous results reported by Boufi and Chaker,[9] who generated CNFs with an average diameter of less than 100 nm from oxidized corn pulp with carboxyl content 480 μmol/g via high-speed blender. However, the variation in diameter was related to the distinct cellulose sources and pre-treatment conditions. It has been known that the dimensions of cellulose fibers are greatly influenced by cellulose sources and pre-treatment conditions.[26,62,63]

3.5. Thermogravimetric Analysis. The thermal stability of SFs, CNFs, and all ACNFs under different acetic anhydride concentrations of 45, 55, and 65 mL was investigated using a TGA. Figure 7a,b depicts the TGA and DTG curves of SF, CNF, and all ACNFs. From the TGA and DTG curves, the onset degradation temperature (T_{onset}), the maximum degradation temperature (T_{max}), and the residual mass value ($W_{residue}$) were obtained and their results are presented in Table 2. As shown in Figure 7a, it can be observed that all

Table 2. Thermal Properties of SF, PSF, CNF, and ACNF

sample	T_{onset} (°C)	T_{max} (°C)	$W_{residue}$ (%)
SF	271.9	348.4	30.5
CNF	308.7	346.0	22.7
ACNF-45	322.1	350.0	21.8
ACNF-55	329.8	351.0	21.3
ACNF-65	319.1	347.5	17.1

samples exhibited three stages of degradation. In the first degradation stage, all samples showed a minor weight loss occurred at room temperature to 120 °C, which was related to the evaporation of absorbed water.[25] In the second degradation step, the crystalline regions disintegrated at around 220−390 °C. The polymer was simultaneously decomposed, resulting in an increase in the amorphous structure and a reduction in the polymerization degree.[12] In the third step, around 390 to 600 °C, the crystal domains were entirely disintegrated, and the cellulose was decomposed into the monomer D-glucopyranose, which could then be decomposed into free radicals.[64]

Table 2 shows that the onset temperatures (Tonset) of SF and CNF were 271.9 and 308.7 °C, respectively. This finding revealed that the CNF had a higher onset temperature than SF. Higher thermal stability shown by CNF compared with the SF was ascribed to the higher C_rI of the CNF as indicated by XRD analysis (Table 2). Furthermore, the higher C_rI of the CNF was related to the removal of amorphous components such as hemicellulose and lignin during the bleaching process using AHP.[65] From Table 2, it was found that the T_{onset} values of the ACNFs with different concentrations of 45, 55, and 65 mL were 322.1, 329.8, and 319.1 °C, respectively. The results indicate that all ACNFs exhibited a much higher T_{onset} than the SF and CNF. In addition, the T_{onset} of ACNFs was increased from 322.1 to 329.8 °C with the increase of acetic anhydride concentration from 45 to 55 mL. The T_{onset} decreased to 319.1 °C when the acetic anhydride concentration was increased to 65 mL. This suggested that the acetic anhydride concentration influenced the thermal stability of ACNF and the optimal acetic anhydride amount was achieved at 55 mL. From Figure 7b and Table 2, it was obtained that the main degradation temperature (T_{max}) for the SF and the CNF was obtained to be 348.4 and 346.0 °C. On the other hand, the T_{max} value for the ACNF-45, ACNF-55, and ACNF-65 were 350, 351, and 347.5 °C, respectively. These findings indicated that the highest T_{max} value of ACNF was obtained for an acetic anhydride of 55 mL. This trend was similar to that of the T_{onset}, showing that the thermal stability of ACNF was also affected by the acetic anhydride concentration. Overall, the acetylation process enhanced the thermal resistance of CNFs. The improvement of thermal resistance was related to the partial removal of amorphous domains such as hemicelluloses and lignin during acetylation.[18] The higher thermal stability was also probably ascribed to the substitutions of hydroxyl groups in cellulose by acetyl groups, which were more stable and produced better thermal resistance.[66] Moreover, the higher thermal stability shown by ACNF was attributed to a higher C_rI, as presented in Table 1. According to Nascimento and Rezende, the enhanced C_rI corresponded to the increased thermal stability of the CNFs.[67] The high crystallinity (orderly arrangement) of cellulose molecules due to the removal of amorphous regions during acid hydrolysis limited heat transfer through the glycosidic chain and thus increased thermal resistance.[68,69] An increase in thermal stability due to acetylation treatment on CNFs was also demonstrated by Ashori et al.[18] The results of this study are different from previous studies,[23] which found that the thermal stability of ACNF was lower than that of CNF. The reduction in thermal stability of ACNF might be attributed to differences in terms of the cellulose sources and the nanofibrillation methods used. Furthermore, both CNF (346 °C) and ACNF-55 (351 °C) demonstrated better thermal stability compared to that of non-acetylated CNF (325 °C) and acetylated CNF (343 °C) reported by Sofla et al.[24] with the same method using a high-speed blender. The increased CNF C_rI in this work may be believed to be the cause of the difference in thermal stability.

From Table 2, it can also be obtained that the residual weight ($W_{residue}$) of SF and CNF was 30.5 and 22.7%, respectively. The $W_{residue}$ value for ACNFs with different acetic anhydride concentrations of 45, 55, and 65 mL was 21.8, 21.3, and 17.1%, respectively. These findings revealed that the SF exhibited the highest $W_{residue}$ value compared to CNF and ACNF. The highest value of the residue was associated with a higher lignin content in the SF compared to that in the CNF and ACNF.[70] It was reported that the lignin content strongly influenced the formation of the fiber char in the fiber.[70] The lower residue content of CNF and ACNF compared to that of SF contributed to the improved thermal stability, mainly owing to the effective dissolving of hemicellulose and lignin in the AHP pre-treatment and acetylation process.[69]

3.6. Water Contact Angle Measurement. The water contact angle was measured to characterize the surface wettability of CNF and ACNF with different amounts of acetic anhydride. Figure 8 depicts the results of the contact angle measurement of the CNF and ACNF with different acetic anhydride amounts. It can be seen from Figure 8a that the contact angle of the CNF could not be measured. The difficulty in measuring the contact angle of CNF was caused by the droplet being completely absorbed by the hydrophilic property of CNF.[24,71] From Figure 8, it can be seen that the contact angle of ACNF at various acetic anhydride amounts of 45, 55, and 65 mL was 30.1 ± 1.50°, 37.7 ± 1.58°, and 40 ± 2.12°, respectively. These results confirmed that the water contact angle of CNF was increased significantly after acetylation. The evolution of the water contact angle of CNF after acetylation suggested that the acetylation process altered

https://doi.org/10.1021/acsomega.3c02178
ACS Omega 2023, 8, 27117−27126

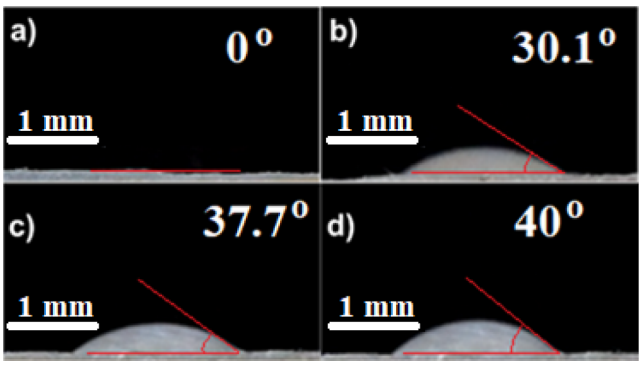

Figure 8. Micrographs of water drop on the surface of CNF and ACNF with different amounts of acetic anhydride: (a) CNF (b) ACNF-45 (c) ACNF-55 (d) ACNF-65.

the nature of the surface of CNFs from highly hydrophilic to more hydrophobic due to the partial replacement of hydroxyl groups with the acetyl groups.[18] The acetylation drastically reduced the water wettability of CNF, indicating that the chemical modification on the surface of CNF occurred.[18] The water contact angle of ACNF-55 (37.7°) is similar to that reported by Ashori et al. but much lower than that reported by Sofla et al. (66°), and Yuan et al. (62°).[18,21,24] The variability in contact angle measurement may be due to process variability and factors such as surface roughness, moisture content, and extractives content of the sample.

From Figure 8, it can also be observed that the water contact angle of ACNFs was increased with increasing the amount of acetic anhydride. This trend was similar to that of the DS, where the increase in the amounts of acetic anhydride increased the DS. This might be because the number of replacements of hydroxyl groups with acetyl groups increases with increasing amounts of acetic anhydride which eventually increased the water contact angle. This finding was consistent with previous studies.[53] Based on the DS and water contact angle results, it was concluded that increasing the amount of acetic anhydride increased DS and water contact angle. In addition, this confirmed that obtained ACNF had higher interface compatibility with non-polar materials.[53] According to Yuan et al., the reduction in ACNF hydrophilicity could enhance the dispersion of CNFs and interfacial adhesion in non-polar polymeric matrixes.[21] It was concluded that the resulting ACNF had great potential as reinforcement material in the nanocomposites using a non-polar polymeric matrix.

4. CONCLUSIONS

The ACNFs with varying acetic anhydride amounts were successfully produced in this study. The characteristics of ACNFs were strongly affected by the amount of acetic anhydride. The ATR-FTIR results indicated successful acetylation of CNFs, while the XRD results demonstrated that the acetylation treatment increased the C_rI of CNFs. The TGA indicated that the acetylation process significantly improved the thermal resistance of CNFs. From the measurement of the water contact angle, it was found that the acetylation process altered the nature of the CNF surface from hydrophilic to more hydrophobic, as indicated by an increase in the contact angle. The optimal amount of acetic anhydride was achieved with 55 mL of acetic anhydride resulting in a C_rI of 77%, a diameter of 87.48 mm, and the best thermal stability. Finally, the resulting ACNFs showed promising potential as a reinforcing agent in nanocomposites with non-polar polymer matrices.

AUTHOR INFORMATION

Corresponding Author

Kusmono − *Department of Mechanical and Industrial Engineering, Faculty of Engineering, Universitas Gadjah Mada, Yogyakarta 55281, Indonesia;* orcid.org/0000-0003-1465-3013; Email: kusmono@ugm.ac.id

Authors

Romi Sukmawan − *Department of Mechanical and Industrial Engineering, Faculty of Engineering, Universitas Gadjah Mada, Yogyakarta 55281, Indonesia; Department of Mechanical Technology, Politeknik LPP, Jalan LPP 1A, Yogyakarta 11840, Indonesia*

Muhammad Waziz Wildan − *Department of Mechanical and Industrial Engineering, Faculty of Engineering, Universitas Gadjah Mada, Yogyakarta 55281, Indonesia*

Complete contact information is available at: https://pubs.acs.org/10.1021/acsomega.3c02178

Author Contributions

R.S.: resources, methodology, investigation, writing-original draft, and revision of the manuscript; K.: conceptualization, supervision, reviewing, and editing; M.W.W.: supervision, reviewing, and editing.

Notes

The authors declare no competing financial interest.

ACKNOWLEDGMENTS

The authors would like to thank the Indonesia Endowment Fund for Education (LPDP) from the Ministry of Finance of the Republic of Indonesia for financial support through a Doctoral scholarship with contract no. KEP-826/LPDP/LPDP.3/2021 to one of us (Romi Sukmawan).

REFERENCES

(1) Ifuku, S.; Nogi, M.; Abe, K.; Handa, K.; Nakatsubo, F.; Yano, H. Surface modification of bacterial cellulose nanofibers for property enhancement of optically transparent composites: dependence on acetyl-group DS. *Biomacromolecules* **2007**, *8*, 1973−1978.

(2) Nogi, M.; Iwamoto, S.; Nakagaito, A. N.; Yano, H. Optically transparent nanofiber paper. *Advanced Materials* **2009**, *21*, 1595−1598.

(3) Bulota, M.; Kreitsmann, K.; Hughes, M.; Paltakari, J. Acetylated microfibrillated cellulose as a toughening agent in poly (lactic acid). *J. Appl. Polym. Sci.* **2012**, *126*, E449−E458.

(4) Nechyporchuk, O.; Belgacem, M. N.; Bras, J. Production of cellulose nanofibrils: A review of recent advances. *Ind. Crops Prod.* **2016**, *93*, 2−25.

(5) Guo, J.; Fang, W.; Welle, A.; Feng, W.; Filpponen, I.; Rojas, O. J.; Levkin, P. A. Superhydrophobic and slippery lubricant-infused flexible transparent nanocellulose films by photoinduced thiol-ene functionalization. *ACS Appl. Mater. Interfaces* **2016**, *8*, 34115−34122.

(6) Belbekhouche, S.; Bras, J.; Siqueira, G.; Chappey, C.; Lebrun, L.; Khelifi, B.; Marais, S.; Dufresne, A. Water sorption behavior and gas barrier properties of cellulose whiskers and microfibrils films. *Carbohydr. Polym.* **2011**, *83*, 1740−1748.

(7) Klemm, D.; Kramer, F.; Moritz, S.; Lindström, T.; Ankerfors, M.; Gray, D.; Dorris, A. Nanocelluloses: a new family of nature-based materials. *Angew. Chem. Int. Ed.* **2011**, *50*, 5438−5466.

(8) Chen, P.; Yu, H.; Liu, Y.; Chen, W.; Wang, X.; Ouyang, M. Concentration effects on the isolation and dynamic rheological

behavior of cellulose nanofibers via ultrasonic processing. *Cellulose* **2013**, *20*, 149−157.
(9) Boufi, S.; Chaker, A. Easy production of cellulose nanofibrils from corn stalk by a conventional high-speed blender. *Ind. Crops Prod.* **2016**, *93*, 39−47.
(10) Josset, S.; Orsolini, P.; Siqueira, G.; Tejado, A.; Tingaut, P.; Zimmermann, T. Energy consumption of the nanofibrillation of bleached pulp, wheat straw and recycled newspaper through a grinding process. *Nord. Pulp Pap. Res. J.* **2014**, *29*, 167−175.
(11) Eichhorn, S. J.; Dufresne, A.; Aranguren, M.; Marcovich, N. E.; Capadona, J. R.; Rowan, S. J.; Weder, C.; Thielemans, W.; Roman, M.; Renneckar, S.; et al. Review: current international research into cellulose nanofibres and nanocomposites. *J. Mater. Sci.* **2010**, *45*, 1−33.
(12) Hu, W.; Chen, S.; Xu, Q.; Wang, H. Solvent-free acetylation of bacterial cellulose under moderate conditions. *Carbohydr. Polym.* **2011**, *83*, 1575−1581.
(13) John, M. J.; Anandjiwala, R. D. Recent developments in chemical modification and characterization of natural fiber-reinforced composites. *Polym. Compos.* **2008**, *29*, 187−207.
(14) Siró, I.; Plackett, D. Microfibrillated cellulose and new nanocomposite materials: a review. *Cellulose* **2010**, *17*, 459−494.
(15) Nogi, M.; Abe, K.; Handa, K.; Nakatsubo, F.; Ifuku, S.; Yano, H. Property enhancement of optically transparent bionanofiber composites by acetylation. *Appl. Phys. Lett.* **2006**, *89*, 233123.
(16) Zhou, X.; Lin, X.; White, K. L.; Lin, S.; Wu, H.; Cao, S.; Huang, L.; Chen, L. Effect of the degree of substitution on the hydrophobicity of acetylated cellulose for production of liquid marbles. *Cellulose* **2016**, *23*, 811−821.
(17) Jonoobi, M.; Mathew, A. P.; Abdi, M. M.; Makinejad, M. D.; Oksman, K. A comparison of modified and unmodified cellulose nanofiber reinforced poly-lactic acid (PLA) prepared by twin screw extrusion. *J. Polym. Environ.* **2012**, *20*, 991−997.
(18) Ashori, A.; Babaee, M.; Jonoobi, M.; Hamzeh, Y. Solvent-free acetylation of cellulose nanofibers for improving compatibility and dispersion. *Carbohydr. Polym.* **2014**, *102*, 369−375.
(19) Trifol, J.; Sillard, C.; Plackett, D.; Szabo, P.; Bras, J.; Daugaard, A. E. Chemically extracted nanocellulose from sisal fibres by a simple and industrially relevant process. *Cellulose* **2017**, *24*, 107−118.
(20) Zimmermann, M. V. G.; Silva, M. P. D.; Zattera, A. J.; Santana, R. M. C. Effect of nanocellulose fibers and acetylated nanocellulose fibers on properties of poly(ethylene-co-vinyl acetate) foams. *J. Appl. Polym. Sci.* **2017**, *134*, 44760.
(21) Yuan, Y.; Liu, H.; Su, J.; Qin, X.; Qi, H. Acetylated cellulose nanofibers fabricated through chemo-mechanical process for stabilizing Pickering emulsion. *Cellulose* **2021**, *28*, 9677−9687.
(22) Diop, C. I. K.; Li, H. L.; Xie, B. J.; Shi, J. Effects of acetic acid/acetic anhydride ratios on the properties of corn starch acetates. *Food Chem.* **2011**, *126*, 1662−1669.
(23) Cheng, L.; Zhang, D.; Gu, Z.; Li, Z.; Hong, Y.; Li, C. Preparation of acetylated nanofibrillated cellulose from corn stalk microcrystalline cellulose and its reinforcing effect on starch films. *Int. J. Biol. Macromol.* **2018**, *111*, 959−966.
(24) Rahimi Kord Sofla, M.; Batchelor, W.; Kosinkova, J.; Pepper, R.; Brown, R.; Rainey, T. Cellulose nanofibres from bagasse using a high-speed blender and acetylation as a pretreatment. *Cellulose* **2019**, *26*, 4799−4814.
(25) Xu, J.; Wu, Z.; Wu, Q.; Kuang, Y. Acetylated cellulose nanocrystals with high crystallinity obtained by one-step reaction from the traditional acetylation of cellulose. *Carbohydr. Polym.* **2020**, *229*, 115553.
(26) Fonseca, A. D. S.; Panthapulakkal, S.; Konar, S. K.; Sain, M.; Bufalinof, L.; Raabe, J.; Miranda, I. P. d. A.; Martins, M. A.; Tonoli, G. H. D. Improving cellulose nanofibrillation of non-wood fiber using alkaline and bleaching pre-treatments. *Ind. Crops Prod.* **2019**, *131*, 203−212.
(27) Bledzki, A. K.; Gassan, J. Composites reinforced with cellulose-based fibres. *Prog. Polym. Sci.* **1999**, *24*, 221−274.
(28) Bismarck, A.; Aranberri-Askargorta, I.; Springer, J.; Mohanty, A. K.; Misra, M.; Hinrichsen, G.; Czapla, S. Surface characterization of natural fibers; surface properties and the water up-take behavior of modified sisal and coir fibers. *Green Chem.* **2001**, *3*, 100−107.
(29) Chaker, A.; Mutjé, P.; Vilar, M. R.; Boufi, S. Agriculture crop residues as a source for the production of nanofibrillated cellulose with low energy demand. *Cellulose* **2014**, *21*, 4247−4259.
(30) Boufi, S.; Gandini, A. Triticale crop residue: a cheap material for high performance nanofibrillated cellulose. *RSC Adv.* **2015**, *5*, 3141−3151.
(31) Barbosa, R. F. S.; Souza, A. G.; Ferreira, F. F.; Rosa, D. S. Isolation and acetylation of cellulose nanostructures with a homogeneous system. *Carbohydr Polym.* **2019**, *218*, 208−217.
(32) Segal, L.; Creely, J. J.; Martin, A. E.; Conrad, C. M. An Empirical Method for Estimating the Degree of Crystallinity of Native Cellulose Using the X-Ray Diffractometer. *Text. Res. J.* **1959**, *29*, 786−794.
(33) Le Normand, M.; Moriana, R.; Ek, M. Isolation and characterization of cellulose nanocrystals from spruce bark in a biorefinery perspective. *Carbohydr. Polym.* **2014**, *111*, 979−987.
(34) Haleem, N.; Arshad, M.; Shahid, M.; Tahir, M. A. Synthesis of carboxymethyl cellulose from waste of cotton ginning industry. *Carbohydr. Polym.* **2014**, *113*, 249−255.
(35) Robles, E.; Urruzola, I.; Labidi, J.; Serrano, L. Surface-modified nano-cellulose as reinforcement in poly (lactic acid) to conform new composites. *Ind. Crops Prod.* **2015**, *71*, 44−53.
(36) de Castro, D. O.; Bras, J.; Gandini, A.; Belgacem, N. Surface grafting of cellulose nanocrystals with natural antimicrobial rosin mixture using a green process. *Carbohydr. Polym.* **2016**, *137*, 1−8.
(37) Goh, K. Y.; Ching, Y. C.; Chuah, C. H.; Abdullah, L. C.; Liou, N. S. Individualization of microfibrillated celluloses from oil palm empty fruit bunch: comparative studies between acid hydrolysis and ammonium persulfate oxidation. *Cellulose* **2016**, *23*, 379−390.
(38) Oun, A. A.; Rhim, J. W. Characterization of carboxymethyl cellulose-based nanocomposite films reinforced with oxidized nano-cellulose isolated using ammonium persulfate method. *Carbohydr. Polym.* **2017**, *174*, 484−492.
(39) Fortunati, E.; Benincasa, P.; Balestra, G. M.; Luzi, F.; Mazzaglia, A.; Del Buono, D.; Puglia, D.; Torre, L. Revalorization of barley straw and husk as precursors for cellulose nanocrystals extraction and their effect on PVA_CH nanocomposites. *Ind. Crops Prod.* **2016**, *92*, 201−217.
(40) Hafemann, E.; Battisti, R.; Marangoni, C.; Machado, R. A. F. Valorization of royal palm tree agroindustrial waste by isolating cellulose nanocrystals. *Carbohydr. Polym.* **2019**, *218*, 188−198.
(41) Su, J. F.; Huang, Z.; Yuan, X. Y.; Wang, X. Y.; Li, M. Structure and properties of carboxymethyl cellulose/soy protein isolate blend edible films crosslinked by Maillard reactions. *Carbohydr. Polym.* **2010**, *79*, 145−153.
(42) Liu, Y.; Liu, L.; Wang, K.; Zhang, H.; Yuan, Y.; Wei, H.; Wang, X.; Duan, Y.; Zhou, L.; Zhang, J. Modified ammonium persulfate oxidations for efficient preparation of carboxylated cellulose nanocrystals. *Carbohydr. Polym.* **2020**, *229*, 115572−118617.
(43) Filho, G. R.; da Cruz, S. F.; Pasquini, D.; Cerqueira, D. A.; Prado, V. d. S.; de Assunção, R. M. N. Water flux through cellulose triacetate films produced from heterogeneous acetylation of sugar cane bagasse. *J. Membr. Sci.* **2000**, *177*, 225−231.
(44) Cerqueira, D. A.; Filho, G.; Meireles, C. D. S. Optimization of sugarcane bagasse cellulose acetylation. *Carbohydr. Polym.* **2007**, *69*, 579−582.
(45) Xie, H.; King, A.; Kilpelainen, I.; Granstrom, M.; Argyropoulos, D. S. Thorough chemical modification of wood-based lignocellulosic materials in ionic liquids. *Biomacromolecules* **2007**, *8*, 3740−3748.
(46) Hu, H.; Li, H.; Zhang, Y.; Chen, Y.; Huang, Z.; Huang, A.; Zhu, Y.; Qin, X.; Lin, B. Green mechanical activation-assisted solid phase synthesis of cellulose esters using a co-reactant: effect of chain length of fatty acids on reaction efficiency and structure properties of products. *RSC Adv.* **2015**, *5*, 20656−20662.

https://doi.org/10.1021/acsomega.3c02178
ACS Omega 2023, 8, 27117−27126

(47) Sun, R.; Fang, J.; Tomkinson, J.; Jones, G. L. Acetylation of wheat straw hemicelluloses in N,N-dimethylacetamide/ LiCl solvent system. *Ind. Crop Prod.* **1999**, *10*, 209−218.
(48) Ishida, K.; Yokota, S.; Kondo, T. Localized surface acetylation of aqueous counter collision cellulose nanofibrils using a Pickering emulsion as an interfacial reaction platform. *Carbohydr. Polym.* **2021**, *261*, 117845.
(49) Hamalainen, C.; Reid, J. D. Decrystallization of cotton cellulose by partial acetylation: Studies on partial acetylation of cotton cellulose (part 1). *Ind. Eng. Chem.* **1949**, *41*, 1018−1021.
(50) Kim, D. Y.; Nishiyama, Y.; Kuga, S. Surface acetylation of bacterial cellulose. *Cellulose* **2002**, *9*, 361−367.
(51) Tripathi, A.; Ago, M.; Khan, S. A.; Rojas, O. J. Heterogeneous acetylation of plant fibers into micro- and nanocelluloses for the synthesis of highly stretchable, tough, and water-resistant co-continuous filaments via wet-spinning. *ACS Appl. Mater. Interfaces* **2018**, *10*, 44776−44786.
(52) Colussi, R.; El Halal, S. L. M.; Pinto, V. Z.; Bartz, J.; Gutkoski, L. C.; da Rosa Zavareze, E.; Dias, A. R. G. Acetylation of rice starch in an aqueous medium for use in food. *LWT-Food Sci. Technol.* **2015**, *62*, 1076−1082.
(53) Duan, L.; Liu, R.; Duan, Y.; Li, Z.; Li, Q. A simultaneous strategy for the preparation of acetylation modified cellulose nanofiber/polypropylene composites. *Carbohydr. Polym.* **2022**, *277*, 118744.
(54) French, A. D. Idealized powder diffraction patterns for cellulose polymorphs. *Cellulose* **2014**, *21*, 885−896.
(55) Ávila Ramírez, J. A.; Gómez Hoyos, C.; Arroyo, S.; Cerrutti, P.; Foresti, M. L. Acetylation of bacterial cellulose catalyzed by citric acid: Use of reaction conditions for tailoring the esterification extent. *Carbohydr. Polym.* **2016**, *153*, 686−695.
(56) Takkalkar, P.; Griffin, G.; Kao, N. Enhanced mechanical and barrier performance of poly (lactic acid) based nanocomposites using surface acetylated starch nanocrystals. *J. Polym. Environ.* **2019**, *27*, 2078−2088.
(57) Souza Da Rosa, T.; Trianoski, R.; Michaud, F.; Belloncle, C.; Iwakiri, S. Efficiency of different acetylation methods applied to cellulose fibers waste from pulp and paper mill sludge. *J. Nat. Fibers* **2022**, *19*, 185−198.
(58) Ponnu Krishnan, P.; Selwin Rajadurai, J. Microscopical, physico-chemical, mineralogical, and mechanical characterization of Sansevieria zeylanica fibers as potential reinforcement of composite structures. *J. Compos. Mater.* **2017**, *51*, 811−829.
(59) Ho, T.; Abe, K.; Zimmermann, T.; Yano, H. Nanofibrillation of pulp fibers by twin-screw extrusion. *Cellulose* **2015**, *22*, 421−433.
(60) Sassi, J. F.; Chanzy, H. Ultrastructural aspects of the acetylation of cellulose. *Cellulose* **1995**, *2*, 111−127.
(61) Jonoobi, M.; Harun, J.; Mathew, A. P.; Hussein, M. Z. B.; Oksman, K. Preparation of cellulose nanofibers with hydrophobic surface characteristics. *Cellulose* **2010**, *17*, 299−307.
(62) Sukmawan, R.; Kusmono; Rahmanta, A. P.; Saputri, L. H. The effect of repeated alkali pretreatments on the morphological characteristics of cellulose from oil palm empty fruit bunch fiber-reinforced epoxy adhesive composite. *Int. J. Adhes. Adhes.* **2022**, *114*, 103095.
(63) Mondragon, G.; Fernandes, S.; Retegi, A.; Peña, C.; Algar, I.; Eceiza, A.; Arbelaiz, A. A common strategy to extracting cellulose nanoentities from different plants. *Ind. Crop Prod.* **2014**, *55*, 140−148.
(64) Yang, Z.; Xu, S.; Ma, X.; Wang, S. Characterization and acetylation behavior of bamboo pulp. *Wood Sci. Technol.* **2008**, *42*, 621−632.
(65) Syafri, E.; Sari, N. H.; Sari, N. H.; Mahardika, M.; Amanda, P.; Ilyas, R. A. Isolation and characterization of cellulose nanofibers from Agave gigantea by chemical-mechanical treatment. *Int. J. Biol. Macromol.* **2022**, *200*, 25−33.
(66) Lin, N.; Huang, J.; Chang, P. R.; Feng, J.; Yu, J. Surface acetylation of cellulose nanocrystal and its reinforcing function in poly(lactic acid). *Carbohydr. Polym.* **2011**, *83*, 1834−1842.
(67) Nascimento, S. A.; Rezende, C. A. Combined approaches to obtain cellulose nanocrystals, nanofibrils and fermentable sugars from elephant grass. *Carbohydr. Polym.* **2018**, *180*, 38−45.
(68) Saurabh, C. K.; Mustapha, A.; Masri, M. M.; Owolabi, A. F.; Syakir, M. I.; Dungani, R.; Paridah, M. T.; Jawaid, M.; Abdul Khalil, H. P. S. Isolation and characterization of cellulose nanofibers from Gigantochloa scortechinii as a reinforcement material. *J. Nanomater.* **2016**, *2016*, 1−8.
(69) Midhun Dominic, C. D.; Maheswary, S.; Neenu, K. V.; Sajadi, S. M.; dos Santos Rosa, D.; Sabura Begum, P. M.; Mathew, M.; Ajithkumar, T. G.; Parameswaranpillai, J.; George, T. S.; Resmi, V. C.; Ilyas, R. A.; Badawi, M. Colocasia esculenta stems for the isolation of cellulose nanofibers: a chlorine-free method for the biomass conversion. *Biomass Convers. Biorefin.* **2022**, DOI: 10.1007/s13399-022-03171-z.
(70) Sethi, S.; Datta, A.; Gupta, B. L.; Gupta, S. Optimization of cellulase production from bacteria isolated from soil. *Int. Sch. Res. Notices* **2013**, *2013*, 1−7.
(71) Kontturi, K. S.; Biegaj, K.; Mautner, A.; Woodward, R. T.; Wilson, B. P.; Johansson, L. S.; Lee, K. Y.; Heng, J. Y. Y.; Bismarck, A.; Kontturi, E. Noncovalent surface modification of cellulose nanopapers by adsorption of polymers from aprotic solvents. *Langmuir* **2017**, *33*, 5707−5712.

https://doi.org/10.1021/acsomega.3c02178
ACS Omega 2023, 8, 27117−27126